Polymer Nanowire Elastic Moduli Measured with Digital Pulsed Force Mode AFM †

ARTICLE *in* LANGMUIR · NOVEMBER 2005

Impact Factor: 4.46 · DOI: 10.1021/la050538o · Source: PubMed

4 AUTHORS, INCLUDING:

Abdullah Alkhateeb Aljaafari
King Faisal University
50 PUBLICATIONS **363** CITATIONS
SEE PROFILE

Eric Aston
University of Idaho
63 PUBLICATIONS **978** CITATIONS
SEE PROFILE

Polymer Nanowire Elastic Moduli Measured with Digital Pulsed Force Mode AFM†

Saravanarajan Shanmugham,‡ Jonghwa Jeong,‡ Abdullah Alkhateeb,§ and D. Eric Aston*,‡

Department of Chemical Engineering, P.O. Box 441021, and Department of Physics, P.O. Box 440903, University of Idaho, Moscow, Idaho 83844-1021

Received February 28, 2005. In Final Form: May 6, 2005

The mechanical bending behavior of polymer nanowires—polypyrrole and poly(3,4-ethylene dioxythiophene-*co*-styrene sulfonate)—produced by template molding were measured using a new innovation in atomic force microscopy (AFM). Digital pulsed force mode (DPFM) was used to image and simultaneously perform three-point bend tests along nanowires spanning microchannels in silicon. The bending profiles were analyzed for apparent elastic moduli variations along the suspended length of individually isolated nanowires and compared to classic beam deflection models for various geometric and boundary conditions. The elastic moduli calculated from these AFM data are 2−7 times that expected for bulk polymer values (∼1−3 GPa), demonstrating an apparent strengthening of nanostructured polymer even for diameters greater than 100 nm—the accepted boundary for nanoscience. Furthermore, detailed analysis of deflection data versus loading location demonstrates the experimental dependence on test geometry and inherent errors in relying solely on midpoint bending measurements or any single loading configuration for nanomechanical testing as well as the significant contribution of nanoindentation effects.

Introduction

Nanowires, sometimes called nanocylinders, nanofibers, nanofibriles, and nanowhiskers, constitute a majority in the family of structures categorized by a high length-to-diameter, or thickness, ratio (perhaps $L/d \geq 20$), where the narrowest dimension is generally of the order of 100 nm or smaller. Variations on the nanowire include the shorter nanobeams and nanorods[1] and objects of noncircular cross section, such as hollow nanotubes[2] and nanotubules,[3] flat nanoribbons,[4] and coiled nanosprings.[5] These nanomaterials are the focus of significant research efforts for their possible applications in microelectronics, nanomechanical actuators, composite separation membranes, and energy storage devices. Nanowires of many kinds may someday provide or replace essential device components, such as the interconnects for micro- and optoelectronics, crossover junctions for switches, artificial composite materials for biomimetic implants, or nanoprobes and biosensors for medical and environmental diagnostics.[6−8] Due to the natural impediments of production-level fabrication at the nanoscale, realistic short-term applications may address improvements in bulk material properties, such as composite strength in fabrics and filler-matrix materials.[9] More detailed and fundamental analyses of the behavior of single nanowires are needed to make the next steps forward in true "nanoengineering" design.

The characterization of a simple mechanical property like bending stiffness or elastic modulus becomes difficult even at the microscale. Atomic force microscopy (AFM) and careful sample preparation make it possible to conduct rudimentary mechanical tests on nanowires and their ilk. Nanomechanical tensile and bending measurements have been accomplished on single-walled (SWNT)[2,10] and multiwalled carbon nanotubes.[1] Walters et al.[10] first deposited a nanotube on a substrate and then etched a microchannel under it for bending. This method is not appropriate for nanowire materials that would be altered or destroyed by the lithography process. Salvetat et al.[2] aligned nanotubes across a microchanneled substrate, which serves better as a general method for all materials. Wong et al.[1] used a different measurement mode, where the nanotube was fixed at one end to the substrate (cantilevered) and bent from the free end, as in lateral force microscopy (LFM). These results did not include correcting for the friction resistance in the measurements.

The first investigations on the mechanics of individual polymer nanotubes[11,12] used compressive indentation against a rigid support to show an apparent increase in elastic modulus as a function of decreasing outer diameter and tube wall thickness. An alternative method to AFM techniques involves the use of an electric field-induced dynamic resonance with in situ TEM.[13,14] However, this

† Part of the Bob Rowell Festschrift special issue.

* Corresponding author. E-mail: aston@uidaho.edu. Phone: 208-885-6793, Fax: 208-885-7462.

‡ Department of Chemical Engineering.

§ Department of Physics.

(1) Wong, W. E.; Sheehan, P. E.; Lieber, C. M. *Science* **1997**, *277*, 1971.

(2) Salvetat, J. P.; Briggs, G. A. D.; Jean-Marc, B.; Revathi, R. B.; Andrzej, J. K.; Thomas, S.; Nancy, A. B.; Laszlo, F. *Phys. Rev. Lett.* **1999**, *82*, 944.

(3) Martin, C. R. *Acc. Chem. Res.* **1995**, *28*, 61.

(4) Samorí, P.; Francke, V.; Müllen, K.; Rabe, J. P. *Thin Solid Films* **1998**, *336*, 13.

(5) McIlroy, D. N.; Alkhateeb, A.; Zhang, D.; Aston, D. E.; Marcy, A. C.; Norton, M. G. *J. Phys.*: *Condens. Matter* **2004**, *16*, R415.

(6) Menon, V. P.; Lei, J.; Martin, C. R. *Chem. Mater.* **1996**, *8*, 2382.

(7) Bayley, H.; Martin, C. R. *Chem. Rev.* **2000**, *100*, 2575.

(8) Kros, A.; van Hovell, S. W. F. M.; Sommerdijk, N. A. J. M.; Nolte, R. J. M. *Adv. Mater.* **2001**, *13*, 1555.

(9) Krishnappa, R. V. N.; Desai, K.; Sung, C. *J. Mater. Sci.* **2003**, *38*, 2357.

(10) Walters, D. A.; Ericson, L. M.; Casavant, M. J.; Liu, J.; Colbert, D. T.; Smith, K. A.; Smalley, K. A. *Appl. Phys. Lett.* **1999**, *74*, 3803.

(11) Cuenot, S.; Demoustier-Champagne, S.; Nysten, B. *Phys. Rev. Lett.* **2000**, *85*, 1690.

(12) Park, J. G.; Kim, B.; Lee, S. H.; Park, Y. W. *Thin Solid Films* **2003**, *438−439*, 118.

(13) Wang, Z. L.; Dai, Z. R.; Gao, R. P.; Bai, Z. G.; Gole, J. L. *Appl. Phys. Lett.* **2000**, *77*, 3349.

(14) Zhang, H. F.; Wang, C. M.; Buck, E. C.; Wang, L. S. *Nano Lett.* **2003**, *3*, 577.

10.1021/la050538o CCC: $30.25
Published on Web 06/11/2005

indirect method is more difficult to accomplish and interpret as compared to traditional three-point bending experiments.

The objectives of this work are to determine elastic moduli of (semi-)conducting polymer nanowires and furthermore to discuss and clarify the issues of variability in testing material properties at the nanoscale. Using the relatively new digital pulsed force mode (DPFM)[15−17] of AFM, three-point bending profiles are recorded over the entire length of end-supported nanowires. This technique provides enough data to resolve the effects of nanowire nonuniformity on single-position measurements and to investigate the validity of boundary condition assumptions used to compute elastic modulus from force−distance curves. Young's moduli for nanowires are computed and compared on a basis of classic mechanics models. Of particular interest is the determination of the diameter range for which nanowires exhibit significant deviations from macroscopic bending strength. Motivations for the study of conducting and semiconducting polymers in particular are the possible applications in flexible electronics and permselective nanosensors as well as for constructing methodologies to test the interrelationships between physicochemical properties of molecular structure, material strength, and electron mobility.

Materials and Methods

Polymer nanowires were synthesized by the common template method.[18−24] Alumina Anodisc templates (25 mm diameter, ∼50 μm thick, Whatman) with average pore sizes of 200, 100, and 20 nm served as the molding environment. Polypyrrole (PPy) nanowires were polymerized inside the template pores from solutions of pyrrole monomer and ferric chloride as an oxidizing agent, both added dropwise to the template. Reagent grade pyrrole (Aldrich Co.) was dissolved in ethanol to 1 M; ferric chloride (Fisher Scientific) was dissolved in deionized water to 0.6 M. In the case of the preexisting polymer, poly(3,4-ethylene dioxythiophene-*co*-styrene sulfonate) or PEDOT-PSS (CAS Registry No. 155090-83-8; Aldrich Co. 48,309-5), the template was loaded dropwise with 0.65 wt % in deionized water.

The filled templates were dried and the alumina dissolved with 2.5 M aqueous sodium hydroxide (Fisher Scientific) to release the nanowires. The resulting suspensions were repeatedly centrifuged, decanted, diluted, and filtered to remove the salts and to isolate clean nanowires. Some nanowires were as long as 60 μm, roughly the template thickness. Templates of all pore sizes were found to produce nanowires largely in the diameter range of 100−250 nm due to the high pore diameter polydispersity and perhaps swelling of the released nanowires. However, the latter is less probable since swelling would then lead to a less dense and therefore weaker nanowire, contrary to our findings.

Submonolayers of nanowires were first deposited from the clean suspensions onto silicon substrates for imaging. They were subsequently transferred to microchannel substrates by physical contact for mechanical testing. Silicon calibration grids with channel widths of 1.5 μm (TGZ-series, MikroMasch) were used as the supports. Nanowires lying perpendicularly across microchannels (Figure 1) were first optically located with the use of high-resolution dark-field microscopy before sample alignment in the AFM. The same nanowires were checked by SEM for diameter variability after mechanical experiments.

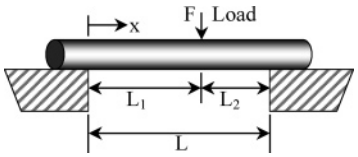

Figure 1. Nanowire bending interpreted by classic point load (F) applied to cylindrical beam fixed at both ends by adhesion.

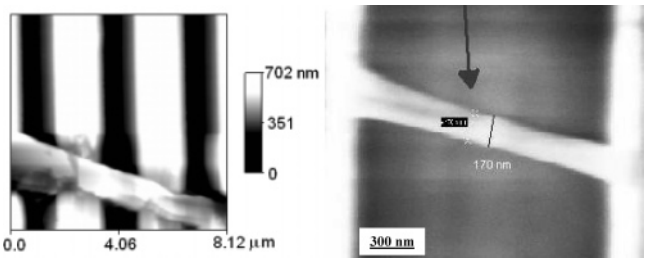

Figure 2. DPFM topography (left) and SEM (right) images of the same PEDOT-PSS nanowire (Ø170 nm, midpoint) aligned across a silicon microchannel.

A Nano-R AFM (Pacific Nanotechnology, Inc.) with closed-loop scanning was used to image and perform the nanomechanical tests with DPFM (WITec, Germany), an electronic advancement over the earlier and more limited pulsed-force mode (PFM) unit.[15] For meaningful quantitative analysis of the nanomechanical results, independent calibrations were first made for the normal cantilever force constants (k_c), AFM scanner and photodetector sensitivities, and the DPFM modulation factor. Arrow cantilevers (NanoWorld) with nominal spring constant of 2.8 N/m and high mechanical quality (Q > 200) were calibrated by resonance frequency sweeps using Sader's method.[25,26] Photodetector sensitivity (actual AFM scanner displacement in nm vs detector response in mV) was determined from standard force−distance profiles acquired on silicon for both loading (approach) and unloading (retract) curves, i.e., constant compliance. The DPFM modulation factor was determined for the experimental amplitude range to provide the most accurate cantilever deflection measurements; this parameter is specific to each AFM.

Digital Pulsed Force Mode. DPFM and PFM provide intermittent contact between probe and sample, operating at frequencies far below mechanical resonance of the cantilever and at modulation amplitudes unrestrained by cantilever resonance behavior. In this slow "tapping" mode with its high-speed data acquisition, the instantaneous cantilever deflection can be monitored in real-time (∼5000 points per μs) during the course of imaging. This deflection-time data set is then available for post-processing to deconvolute local surface properties associated with each topographic pixel in a DPFM image. For best results, the AFM scan rates and PFM frequency should be correlated to give two or more complete oscillations per pixel. The data set is then segmented into single cycles. These data are converted into the more useful applied force versus nanowire deformation curves with the above-calibrated parameters. In this fashion, the mechanical three-point bend tests are collected simultaneously with topography and the on-line, semiquantitative maps of stiffness and adhesion. This effectively eliminates the uncertainty involved in traditional force−distance profiling by correlating precise topographic location with the material properties of interest, specifically here, visco-elastoplasticity.

Results and Discussion

Nanowire Probing. DPFM topography (Figure 2) is compiled from the scanner positions recorded at the set

(15) Krotil, H. U.; Stifter, T.; Waschipky, H.; Weishaupt, K.; Othmar, M.; Hild, S. *Surf. Interface Anal.* **1999**, *27*, 336.
(16) Marti, O.; Stifter, T.; Waschipky, H.; Quintus, M.; Hild, S. *Colloids Surf., A* **1999**, *154*, 65.
(17) Kunneke, S.; Kruger, D.; Janshoff, A. *Biophys. J.* **2004**, *86*, 1545.
(18) Martin, C. R. *Chem. Mater.* **1996**, *8*, 1739.
(19) Cepak, V. M.; Hulteen, J. C.; Che, G.; Jirage, K. B.; Lakshmi, B. B.; Fisher, E. R.; Martin, C. R.; Yoneyama, H. *Chem. Mater.* **1997**, *9*, 1065.
(20) Martin, C. R.; Mitchell, D. T. *J. Electroanal. Chem.* **1999**, *21*, 1.
(21) Hulteen, J. C.; Chen, H. X.; Chambliss, C. K.; Martin, C. R. *Nanostructured Mater.* **1997**, *9*, 133.
(22) Yu, S.; Li, N.; Wharton, J.; Martin, C. R. *Nano Lett.* **2003**, *3*, 815.
(23) Che, G.; Lakshmi, B. B.; Martin, C. R.; Fisher, E. R.; Ruoff, R. S. *Chem. Mater.* **1998**, *10*, 260.
(24) Martin, C. R. *Adv. Mater.* **1991**, *3*, 457.
(25) Sader, J. E.; Chon, J. W. M.; Mulvaney, P. *Rev. Sci. Instrum.* **1999**, *70*, 3967.
(26) Sader, J. *Atomic Force Microscope Cantilevers* (*Calibration Method of Sader*); Department of Mathematics and Statistics, University of Melbourne Website, 2004.

point of maximum force applied by the AFM, which corresponds to the peaks in each cycle of the cantilever modulation. The image of a PEDOT-PSS nanowire in Figure 2 is blurred by these oscillations since the nanowire is free to move except at the supported ends, where it is then compressed against the rigid substrate. The electron micrograph is also blurred because the sample was not sputter-coated, which allows DPFM measurements to be repeated after SEM imaging. Thus, the nanowire appears both wider and flatter under DPFM than expected from SEM, even though the nanowire remains flattened at the supported edges long after the AFM experiments. This static deformation is maintained by strong adhesion and was most likely caused by the contact transfer process. Therefore, mechanical boundary conditions of fixed or clamped ends may be applied to beam bending models[27] for data interpretation. This will provide conservatively low estimates for elastic modulus (E) since a simply supported, stick-slip, free-sliding, or limited-torque end (or two ends) would yield even larger calculated values for E—in the extreme case (simple support) by a factor of 4.

Taken in concert, SEM and tapping mode AFM images roughly indicate conservation of cross-sectional area from a free section of the nanowire to the flatter, elliptical cross section, in support of an elastic assumption. For example, one nanowire from a 100-nm mold showed an average height of 37 nm (based on histogram image analysis) and a full width at half-maximum of 260 nm. A combination of nanowire adhesion and applied force with the AFM tip causes radial compression by a factor of ~2.5. The first conclusion might be that the nanowire is in fact a hollow nanotubule. While this remains a possibility requiring future study, the probability is low in light of the bending data discussed below. Because the moment of inertia for a tube is smaller than for a cylinder of the same outer diameter, the effective moduli calculated from DPFM data would be even larger, in contrast with previous results for nanotubes in this diameter range.[11,12] Therefore, restricting the present analysis to a solid cylinder will again provide conservative (low) estimates for E if the nanowire is hollow, swollen, or spongy.

Scan Rate Dependence and Hysteresis. It has already been shown that AFM measurements of E for thin polymer films can exhibit rate-dependent behavior.[28] While this is an anticipated issue for DPFM, our experiments showed no deflection response variations for repeated measurements on the same nanowire at standard operating conditions of 1 kHz and 500 Hz for cantilever modulation. However, close analysis of individual force-curves reveals some energy loss during deflection, evident from slight hysteresis between loading and unloading slopes. It is not dependent on frequency, suggesting that it may be a function of the experimental geometry. This kind of hysteresis is indicative of the horizontal AFM scan rate coupling with the vertical cantilever displacement during the contact portion of the PFM cycle. This produces minor torsional and shear effects to the cantilever and sample, respectively.

The DPFM data acquired along the centerline of the nanowire are analyzed to minimize experimental error from bending displacements out of the normal plane, since only vertical displacements are measured with DPFM. The effective spring constants of the cantilever-nanowire system (k_{sys}) were measured from the unloading profiles as a function of tip position relative to the edges of the microchannel, L_1 or L_2 (Figure 1). This reduces measurement error due to local plastic deformation of the sample. The unloading, or retracting, curve allows stiffness to be measured in the limit of zero stress, where probe-nanowire adhesion extends the compliance curve below zero applied force. The forces of adhesion maintain tip contact for small, negative applied loads, pulling the nanowire upward and inverting from a compressive to a tensile stress mode on the loaded (top) side. This allows investigation of mechanical hysteresis between downward and upward three-point bending, unique to nanoscaled systems. In the present experiment, the data below zero force were too sparse for definitive comparisons.

Three-Point Bend Tests. The bending spring constant of the polymer nanowire (k_n) is determined from analysis of springs in series, $k_n = k_{sys}k_c/(k_c - k_{sys})$. From this, we find that the effective spring constant of these nanowires are of the same order of magnitude as the cantilevers used, which is optimal for making the most accurate measurements of both applied force and sample deflection. For the PEDOT-PSS nanowires, the experimental range of k_n was 2.8−6.9 N/m, increasing from the midpoint to the edges, as expected. Similarly for PPy, k_n was in the range of 3.2−7.6 N/m. On the supported ends, the values of k_{sys} are larger because only indentation occurs; no bending is possible. Moving off the support end toward the midpoint shows a gradual shift from indentation-dominated deflection to bending-dominated deflection. This inherent variability is unavoidable in three-point bend tests for compliant solids.

A nanowire suspended across a gap of width (L) is bent by a force (F) applied at a point with the AFM cantilever (Figure 1). The classic deflected profile of a beam, $z(x)$, under elastic deformation caused by a vertical point load (ignoring local indentation) at a distance L_1 from one edge is represented by the following:[27,29,30]

$$z = \frac{F}{6EI}\left[L_2^2 x^3 \frac{(L + 2L_1)}{L^3} - \frac{3L_1 L_2^2 x^2}{L^2}\right]$$

AFM provides only paired measurements of z and F at the location where $x = L_1$ and $L_2 = L - L_1$. The cross-sectional moment of inertia for the nanowire has two reasonable forms: $I = \pi d^4/64$ for circular cross section with diameter, d; $I = \pi ab^3/4$ for elliptical cross section, where a and b are the radii in the horizontal (surface) and vertical (bending) planes, respectively. Classic modeling proceeds under the conventional assumptions of constant cross section and of deformations constrained to the elastic limit, where $L/d \approx 10$ and $L/z > 10$.

The suspended nanowire length (L) is measured exactly from AFM and SEM data in each case to account for the deviation from orthogonal alignment with the channel edge. As seen with SEM, the cross section of the nanowire varies from a cylinder in the middle to elliptical near the supported edges. Nanowire thickness was estimated to be 146 nm at the midpoint (a = 85 nm, b = 73 nm) with SEM at a sample rotation of 87° from that in Figure 2. Some error in calculated E values is due to geometrical variations, which cannot be precisely accounted for. However, in all cases, the elastic modulus inferred from

(27) Timoshenko, S. *Strength of Materials*: *Part I* (*Elementary Theory and Problems*), 3rd ed.; Robert E. Krieger Publishing Co.: Huntington, 1976.

(28) Shulha, H.; Kovalev, A.; Myshkin, N.; Tsukruk, V. V. *Eur. Polym. J.* **2004**, *40*, 949.

(29) Young, W. C.; Budynas, R. *Roark's Formula for Stress and Strain*; McGraw-Hill: New York, 2002.

(30) Pilkey, W. D. *Formulas for Stress, Strain, and Structural Matrices*; John Wiley & Sons: New York, 2004.

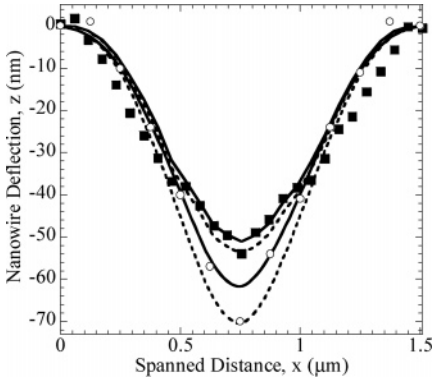

Figure 3. PEDOT-PSS (■) and PPy (○) nanowire bending data from DPFM, fitted for mid-beam (solid lines, E_{beam}) and midpoint only (dashed lines, E_{mid}) deflections. PEDOT-PSS: cylindrical E_{beam} = 6.7 GPa, E_{mid} = 6.4 GPa (d = 170 nm); elliptical E_{beam} = 10.6 GPa, E_{mid} = 10.0 GPa ($a = d/2$, b = 73 nm). PPy: cylindrical E_{beam} = 6.3 GPa, E_{mid} = 5.7 GPa (d = 176 nm); elliptical E_{beam} = 11.0 GPa, E_{mid} = 10.0 GPa ($a = d/2$, b = 73 nm).

a point measurement is mechanically averaged over the entire length of the nanowire.

Uniform Elastic Modulus and Cross Section. Figure 3 shows that if E were determined from a midpoint deflection alone (E_{mid})—the common, quick method—that the mechanical behavior of the nanowire is misrepresented, underestimating the modulus. Even calculating E based on an average profile fit oversimplifies the experimental situation. Using several mid-beam data points shows better agreement between the fitted and experimental profiles. Mid-beam modulus results excluding the midpoint, E_{beam}, are generally 5−6% higher than E_{mid} in this study. The inclusion of measurements from several physically different locations provides an inherent averaging and greater certainty in the result. Restricting the model to load points away from the supported ends further minimizes nonideal edge effects and mechanical variance caused by the changing cross section. Though the bending profile is fairly symmetric from midpoint to edge, the general trend is flatter toward the edges than a constant cross-sectional area predicts.

Continuing this series of modeling, estimates of the expected effects for different values of d and a/b were computed for uniform E, that is, invariant to load location. These transverse dimensions of the nanowire model are essentially effective "mechanical" diameter (model 1) and elliptical radii (model 2), respectively. Since the only difference in these two models is the cross-sectional moment of inertia, the best-fitted curves for each will be identical in shape. These parameters provide a straightforward interpretation for experimental deviations without the detailed analysis of a variable beam cross section, which will be the focus of future computational studies. The contribution of nanoindentation on the measurements must first be quantified with certainty. For the present work, all reported model values of diameter and radii are effective mechanical averages based on theoretical uniform cross sections.

As a first-order correction for the deformation due to nanoindentation of the polymer, the average indentation depth measured on the supported ends of the nanowire was subtracted from the entire data set. This experimental offset is most likely an over-correction that will exaggerate computed values of E. However, even when E is calculated without the necessary indentation offset, for a uniform cylinder (model 1), and based solely on the (conservative) midpoint deflection, E is still slightly larger than expected

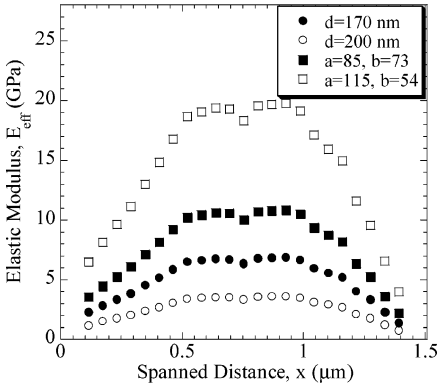

Figure 4. Variation of E fitted for each loading point across PEDOT-PSS nanowire with uniform "mechanical" diameter (● and ○, model 3) or radii a and b (■ and □, model 4).

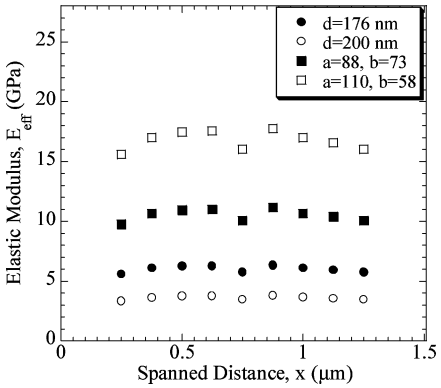

Figure 5. Variation of E fitted for each loading point across PPy nanowire with uniform "mechanical" diameter d (● and ○, model 3) or radii a and b (■ and □, model 4).

(e.g., 2.5 GPa for PEDOT-PSS).[11] The more accurate elliptical nanobeam model is arguably a better geometric fit and provides a greater value of 4.0 GPa (model 2). The average effect of the nanowire flattening out toward the two ends increases both estimates. For example, if a = 90 nm and b = 68.9 nm (to maintain constant cross-sectional area), the result becomes 4.4 GPa. This margin of uncertainty is well within the experimental errors.

Preliminary nanomechanical tests were also completed for a PPy nanowire 176 nm in apparent diameter at the midpoint and 146 nm thick (b = 73 nm). The results obtained from the application of the above models (Figure 5) show similar trends to PEDOT-PSS. For the midpoint cylinder calculation before indentation correction, the modulus was estimated at 2.3 GPa, and the more reasonable elliptical model gave 3.9 GPa. The nanoindentation depth as measured at the supported ends of the nanowires was again subtracted and shows a significant shift in E. This supplies an upper bound on the magnitude of error.

These initial calculations are sufficient evidence for an increase in E over the bulk expectation, even when the effect of nanoindentation is not subtracted. The offset is also an oversimplification since it is not merely an additive phenomenon to bending along the suspended length. At the largest observable nanowire width (Figure 2), model 1 (d = 230 nm) yields an expected bulk modulus of 1.9 GPa (0.75 GPa, uncorrected). Clearly, a 230 nm diameter is far too large, and again the better geometrical fit is provided with model 2 for the extreme dimensions (a = 115, b = 54) giving E = 18.4 GPa (E = 7.2 GPa, uncorrected). Even ignoring indentation, these polymer nanowires are stronger than expected.

Table 1. Elastic Moduli Calculated for Nanowires from DPFM Bend Tests

	PEDOT E (GPa)	PPy E (GPa)
bulk	~2−3	~1−2
raw midpoint	2.5	2.3
model 1	6.7 (6.4)	6.3 (5.7)
model 2	10.6 (10.0)	11.0 (10.0)
model 3	1.4−6.8	5.6−6.4
model 4	2.2−10.8	9.8−11.1

The bending behavior far inside the supporting edges follows the theoretical trend for three-point bending, except for the single anomalous midpoint. This point of largest beam deflection has the highest probability of falling outside of the elastic regime. The local stress and strain, which are the parameters of greatest importance in determining if the true elastic limit has been reached, cannot be precisely measured here. However, the maximum ideal strains experienced by the nanowires during AFM testing, based on geometric arguments, are 1.6% and 2.7% for PEDOT-PSS and PPy experiments, respectively. Considering the maximum force (~800 nN) at an estimated AFM tip contact area (~250 nm^2) gives a localized stress of approximately 3 GPa, suggesting that plastic deformation or yielding could be a contending issue. Bulk elastic moduli for polystyrenes and polypyrrole are 2−3 GPa[31] and 1−2 GPa,[11,32] respectively.

Variable Modulus and Cross Section Effects. Conversely, model 3 applies a uniform mechanical diameter and adjusts E as a function of location: $E_{eff} = E(x)$, an effective modulus mechanically averaged over the bending length. Finally, the finer effects of nonuniformities in elliptical cross section are studied parametrically for changes in horizontal and vertical radii a and b (model 4). Estimated trends of Young's modulus for PEDOT-PSS nanowires are plotted in Figure 4 for the extreme cases, that is, the smallest and largest observable nanowire widths. While the bending behavior will be most accurately described by some set of intermediate parametric values, this plot makes the very significant point of the risk in limited data collection versus the geometric conditions.

A concise comparison of the modeling results are made in Table 1 with respect to the elastic modulus range for the bulk polymers and to the values of E calculated from the raw deflection data for midpoint loading without indentation or cross section corrections. The "raw midpoint" values were calculated for a uniform cylinder and fall within the expected bulk range. This demonstrates a coincidence of self-canceling behavior that leads to the erroneous results. Clearly, the nanowires were not uniform and nanoindentation by the AFM tip was of the same order of magnitude as the bending deformation. Furthermore, the range of variability in E with load location is roughly an order of magnitude, spanning both above and below the bulk values.

Higher elastic moduli in polymer nanowires as compared to bulk values can be attributed to one or more of the following. A lower number or density of stress concentrators (i.e., defects) is a strong argument based solely on statistical averages for smaller volumes. Diffusion-limited transport of monomers (in the PPy case) into the template pores imparts a degree of preferred polymer chain growth and ordering in the long-axis direction. This argument is much weaker for the PEDOT-PSS nanowires. Whether cause or effect, increased π-conjugation may also correlate with nanowire strength for these highly conjugated polymers.[11] Indirect observation of nanowire growth proceeding from the pore walls inward also suggests interfacial chemistry alters the deposition process, inducing nanoscaled property changes.[3] Other considerations are the effects of polymer chain length—difficult to determine due to a dearth of good solvents—and the extent of intra- and intermolecular steric behavior. Cross-linking and branching are not issues for these particular macromolecules.

Conclusions

The quantitative use of digital pulsed force mode AFM has facilitated the demonstration of classic three-point bend tests for profiling variations in mechanical behavior along nanowires, which is readily extended to nanotubules and nanosprings. Relative deviations in bending strength along the nanowire main axis as a result of nonuniformities in cross-sectional area greatly reduce the certainty in estimates of elastic modulus. Polymer nanowires made from template molding showed an increase in bending strength over their bulk counterparts by a factor of 2−7, based on conservative fixed-end bending models. If the true edge-supports allowed for any margin of limited slip or torque, the calculated values for E would be even larger. It is particularly noteworthy that the increase and variability in bending strength was observed for both nanowires polymerized in situ and those produced by templating with preexisting polymer.

Reliance on a blind, single midpoint deflection—even across multiple samples and with repeated measurements—can result in significant error, especially for soft polymeric materials. The evaluations of effective moduli substantiate the need for conducting nanomechanical studies as a function of applied force location with respect to the test geometry and beam support before precise investigations of true local property variation can be pursued in earnest. Furthermore, these experimental findings and the simple mechanical models presented call for the development of a more detailed, predictive model for three-point bending that accounts for the effects of arbitrary cross-sectional variation along the length of a nanowire and limited sliding or bending at the edges. We hope that higher resolution DPFM data near the edges will allow definitive interpretation of the true boundary conditions.

For polymers and other soft materials, a complete mechanical model must also include nanoindentation contributions followed by a thorough nanoindentation study of nanowires fully supported on rigid substrates, independent of three-point bending. In the future, we will also pursue temperature-dependent mechanical measurements to investigate thermal and residual stress effects[33] as well as a greater range of applied forces, deformations, and time scales to probe for strain hardening[34] and other energy loss modes.

Acknowledgment. The authors gratefully acknowledge support of the National Science Foundation (EPS0132626), the W. M. Keck Foundation, and the Idaho Research Council for funding this work.

LA050538O

(31) Green, D. W. *Perry's Chemical Engineers' Handbook*, 6th ed.; McGraw-Hill: New York, 1984.

(32) Andrews, R. *Synthesis and Processing of Nanotube Composite Materials*; Center for Applied Energy Research, University of Kentucky, Lexington, Website, 2004.

(33) Turnbull, A.; Maxwell, A. S.; Pillai, S. *J. Mater. Sci.* **1999**, *34*, 451.

(34) Tervoort, T. A.; Govaert, L. E. *J. Rheol.* **2000**, *44*, 1263.